

Exact and Numerically Stable Expressions for Euler-Bernoulli and Timoshenko Beam Modes

Firas A. Khasawneh* and Daniel Segalman†
 Department of Mechanical Engineering
 Michigan State University

Abstract

In this work we present a general procedure for deriving exact, analytical, and numerically stable expressions for the characteristic equations and the eigenmodes of the Timoshenko and the Euler-Bernoulli beam models. This work generalizes the approach recently described in Gonçalves et al. (P.J.P. Gonçalves, A. Peplow, M.J. Brennan, Exact expressions for numerical evaluation of high order modes of vibration in uniform Euler-Bernoulli beams, *Applied Acoustics* 141 (2018) 371–373), which allows the numerical stabilization for the case of the Timoshenko beam model. Our results enable the reliable computation of the eigenvalues and the eigenmodes of both beam models for any number of modes. In addition to presenting the necessary details for stabilizing the solutions to the eigenvalue problem for the two beam models, we also tabulate the results for a large number of the common boundary conditions so that one can compare the predictions of all those models. Therefore, another contribution of our work is the presentation of both the conventional as well as the novel, numerically stabilized results for both the Euler-Bernoulli and the Timoshenko beam models in one manuscript with consistent notation, and for the most common boundary conditions. The code for the stabilized Timoshenko expressions as well as for the finite element verification are made available through the Mendeley Data repository <http://dx.doi.org/10.17632/r275tx2yp8.1>.

1 Introduction

The elastic deformation of continuous bodies can generally be studied using the theory of elasticity. However, when certain loading conditions are applied to special structural elements, it is possible to simplify the analysis by utilizing the kinematics of the deformation and making some assumptions on the resulting strains. One example of these simplifications is the beam structural element which has been widely used to model a variety of natural and engineered components [1, 2, 3, 4]. Several assumptions must be made when going from the full theory of elasticity to a beam model. These assumptions yield different mathematical models for the same system whose validity often depends on the geometry of the element and the frequency of excitation [5]. Some of the classical beam theories as well as the associated key assumptions are shown in Table 1. From this table it is evident that the most inclusive classical beam model is the Timoshenko beam.

In contrast to the most commonly used Euler-Bernoulli (EB) beam model, the Timoshenko beam (TB) model [6] includes shear and rotary inertia effects in addition to bending deformation and linear inertia. This makes the TB model especially more accurate for beams with smaller length to diameter ratio or with high-frequency excitation where these effects are not negligible and thus using the EB model would yield inaccurate results [7]. Although the TB model gives more accurate results than EB, this improvement in accuracy is associated with a more complicated analysis. This is because there are two degrees of freedom intrinsic to the TB model: lateral translation and cross-section rotation while the EB model has lateral translation as the only degree of freedom. Mathematically, TB consists of two second order coupled partial differential equations (PDEs) [6] while EB consists of one PDE. The two TB equations can be combined into a hyperbolic PDE while the EB equation is a parabolic PDE. This difference causes the TB model to

*khasawn3@egr.msu.edu

†segalman@egr.msu.edu

have two different sets of expressions for the natural frequencies and mode shapes, thus leading to a second spectrum for the TB model [8, 9, 10]. For simple boundary conditions, the TB solutions, natural frequency equations, and mode shapes were derived in [11]. However a correction for the clamped-clamped frequency equations that appeared in [11] was later published in [12]. While analytically these terms are correct, they generally are not suitable for numerical computations. This hinders the analysis of a wide class of systems since beam modes are still regularly used in assumed modes analysis. Therefore, achieving an accurate and numerically stable representation, especially in the much less studied TB models, will be extremely beneficial.

Specifically, it was discovered early on [13] that numerical evaluation of higher mode shapes of many EB beam modes (such as those with clamped or free boundary conditions) can be numerically unstable—in the sense that evaluation of the standard forms of the equations for those modes involves substantial floating point error. Dowell [14] provided an asymptotic form for the high order modes that circumvented the problem of numerical instability. Shankar and Keane [15] restructured the equations for the free-free EB beam so as to isolate the problem to a single term consisting of a very small number multiplying a very large one. Using this approach, they were able to numerically evaluate the first hundred modes for an EB free-free beam. Tang [16] also rearranged the terms of the mode shapes, but did so in a way that reduces catastrophic cancellations which are numerical errors caused by taking the difference of nearly identical terms. However, his formulation still involved taking differences of very large numbers and the core problem persisted. Van Rensburg et al [17] studied the Timoshenko beam model for pinned-pinned and cantilever boundary conditions. While the expressions they provide for the modes are numerically unstable, they derive asymptotic expressions that can be used to approximate the eigenvalues for the two boundary condition cases they considered.

Gonçalves et al [18] rearranged the mode equations for common EB boundary conditions in a manner similar to that done by Shankar and Keane [15]. Similar to [15], they presented exact terms for numerically computing the mode shapes up to the 200th term, and provided approximate terms for modes higher than 200 but at the cost of losing some accuracy at the lower modes. In a recent publication [19], Gonçalves et al presented an exact formulation for the mode shapes of uniform EB beams subject to common boundary conditions. In contrast to their earlier publication [18], the expressions in [19] are exact and numerically stable for the full frequency range where the EB beam theory is valid. The same authors provide a strategy for numerically stabilizing the characteristic frequency equation.

The issue of numerical stability of modes is even more prominent for stepped beams, both Euler-Bernoulli and Timoshenko, where fewer than 10 modes can be predicted reliably [20, 21]. Xu et al. [20] and Cao et al [21] have mitigated the issue by defining a set of local coordinates that decrease the growth rate of the hyperbolic sine and cosine terms in Euler-Bernoulli and Timoshenko beams, respectively. However, their approach does not solve the core problem and numerical stabilities continue to be a problem in their formulation.

Therefore, the problem of obtaining closed form expressions for the mode shapes that are well-conditioned for the whole span of the beam and throughout the frequency range is still a current problem especially for the Timoshenko beam model.

While finite element can be used to obtain eigenfrequencies and mode shapes, analytic expressions are still useful for gaining an understanding of the character of the solution, particularly asymptotic behavior. Additionally, analytic expressions (when they can be evaluated) are necessary to gain confidence in numerical methods such as finite elements (mesh convergence, code validation, etc.). Therefore, closed form and numerically stable solutions for the eigenvalue problem of beams comprise an important analysis tool.

Further, for Timoshenko beams numerical instability occurs at the lower modes which get singular. Therefore, even using a dozen of modes for analyzing the vibrations of these beams can be problematic. On the other hand, for the Euler-Bernoulli beam the number of singular modes depends on the problem, while how many of these modes one needs depends on the application. Civil engineering applications often utilize lower modes; however, mechanical engineering applications often require considering higher modes. For instance, if one is using the assumed modes method it is common to utilize several tens of modes. Consequently, the lack of numerically stable expressions can hinder the analysis of Euler-Bernoulli and Timoshenko beams.

In this paper we present an approach for the numerical stabilization of both the characteristic equation and the modes of the Timoshenko beam model. We present the approach and tabulate the results for a wide range of common boundary conditions. For completeness, we also present the results for the EB model,

where our formulation is mathematically equivalent to the one presented in [19]. We are motivated by both (1) the importance of obtaining numerically stable expressions for the TB model, and (2) the need for presenting EB and TB results in one consistent notation and for all the common boundary conditions in one manuscript. Figure 1 shows the boundary conditions used in this paper. All the combinations of these boundary conditions are considered and the corresponding results are tabulated.

This paper is organized as follows. In Sections 2 and 3 the equations of motion for the EB and the TB models, respectively, are non-dimensionalized and the corresponding mode equations are derived. The source of the numerical instability in the characteristic equations and the mode shape expressions are described in Section 5. Numerically stable expressions for both EB (Section 6.2) and TB (Section 6.3) models, including some useful identities are presented in Section 6. (An expanded discussion of the pinned-pinned case of a TB is presented in B.) Section 7 shows the results obtained using the well-conditioned expressions. Section 8 outlines the use of finite element analysis to verify the exact solutions derived above and a more complete discussion of the finite element analysis and the verification process is presented in D. The paper ends with conclusions in Section 9. Two additional appendices are also provided: A provides more details on mode derivations, while C includes the numerically stable expressions for all the roller boundary condition combinations.

In the following, the nomenclature of [17] is used with the exception that the shear coefficient is represented as κ rather than κ^2 . The authors of this monograph performed their derivations for exact and numerically stable solutions for Euler Bernoulli and Timoshenko beams before [19] was published, so the following will employ the formalism of the authors' derivation.

	Shear deformation	Bending deformation	Linear inertia	Rotary inertia
Euler-Bernoulli	✗	✓	✓	✗
Rayleigh	✗	✓	✓	✓
Shear	✓	✗	✓	✗
Timoshenko	✓	✓	✓	✓

Table 1: Beam models. A check mark in any column means that the factor stated in the header of the column is included in the model, while a cross means that the effect of that factor is neglected.

2 The general eigenvalue problem for the Euler-Bernoulli beam

The lateral vibrations w of a uniform Euler-Bernoulli beam are governed by the partial differential equation

$$EI \frac{\partial^4}{\partial x^4} w = -\rho A \frac{\partial^2}{\partial t^2} w, \quad (1)$$

where ρ is the density, A is the area of cross-section, E is Young's modulus, and I is the area moment of inertia of the cross section about the neutral axis. The beam has length L , and we use the non-dimensional parameters

$$\tau = t/T_E, \quad \zeta = x/L$$

where $T_E = L\sqrt{\rho/E}$. The dimensionless displacement is

$$\tilde{w}(\zeta, \tau) = w(\zeta L, \tau T_E)/L$$

These can be used to derive the following expressions

$$\frac{\partial^4 w}{\partial x^4} = (1/L^3) \frac{\partial^4 \tilde{w}}{\partial \zeta^4} \quad \text{and} \quad \frac{\partial^2 w}{\partial t^2} = (L/T_E^2) \frac{\partial^2 \tilde{w}}{\partial \tau^2}. \quad (2)$$

Substituting the above into Eq. (1) gives

$$\frac{1}{\alpha} \frac{\partial^4 \tilde{w}}{\partial \zeta^4} = -\frac{\partial^2 \tilde{w}}{\partial \tau^2}. \quad (3)$$

where $\alpha = AL^2/I$. We appeal to separation of variables: $\tilde{w}(\zeta, \tau) = U(\zeta)Y(\tau)$ and obtain

$$\frac{\frac{1}{\alpha} \frac{\partial^4 U}{\partial \zeta^4}}{U} = -\frac{\frac{\partial^2 Y}{\partial \tau^2}}{Y} = \lambda, \quad \text{where } \lambda \text{ is assumed positive.} \quad (4)$$

Dimensionless eigenvalue λ is related to physical quantities by $\sqrt{\lambda} = T_E \hat{\omega}$ where $\hat{\omega}$ is the physical natural frequency predicted by the model. We are now interested in the form of U , so we examine the equation

$$\frac{\partial^4 U}{\partial \zeta^4} = \alpha \lambda U. \quad (5)$$

Assuming $U = e^{\mu \zeta}$ and substituting it into the above equation gives

$$e^{\mu \zeta} (\mu^4 - \alpha \lambda) = 0, \quad \text{so } \mu = (\alpha \lambda)^{\frac{1}{4}}. \quad (6)$$

Considering of both real and imaginary roots yields the following real expressions for the general form for the Euler-Bernoulli modes

$$u(\xi) = A_1(\mu) \sinh(\mu \xi) + A_2(\mu) \cosh(\mu \xi) + A_3(\mu) \sin(\mu \xi) + A_4(\mu) \cos(\mu \xi), \quad (7)$$

where the constants A_1 through A_4 depend on the boundary conditions. The most common boundary conditions for the Euler-Bernoulli beam are similar to the ones shown in Fig. 1, and the corresponding mathematical expressions are listed in Table 2.

Condition Name	Equation 1	Equation 2
Cantilever	$u = 0$	$u' = 0$
Simply Supported	$u = 0$	$u'' = 0$
Free	$u'' = 0$	$u''' = 0$
Roller	$u' = 0$	$u''' = 0$

Table 2: The four standard boundary conditions for the Euler-Bernoulli beam.

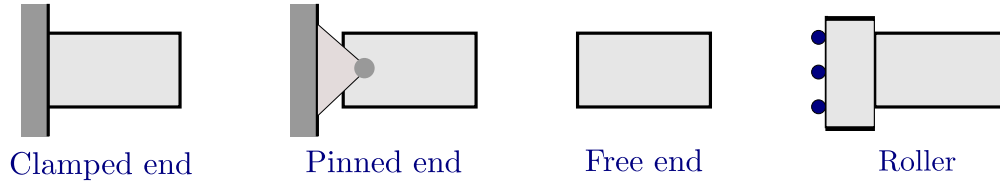


Figure 1: Common beam boundary conditions.

3 The general eigenvalue problem for the Timoshenko beam

The Timoshenko beam model is given by the two coupled partial differential equations [17]

$$\rho A \frac{\partial^2 u}{\partial t^2} = \frac{\partial (AG\kappa(\frac{\partial u}{\partial x} - \phi))}{\partial x}, \quad (8)$$

$$\rho I \frac{\partial^2 \phi}{\partial t^2} = AG\kappa(\frac{\partial u}{\partial x} - \phi) + \frac{\partial (EI \frac{\partial \phi}{\partial x})}{\partial x}, \quad (9)$$

where u is the lateral deflection, ϕ is the angle of rotation of the beam's cross-section, A , E and I have the same meaning described in Section 2, κ is the shear coefficient which corrects for the variation in shear along the cross section due to shear deformation in the Timoshenko beam model [22], while G is the shear modulus. In order to derive these equations, and incorporate the appropriate boundary conditions, the following expressions for the bending moment and the shear force were used

$$M = EI \frac{\partial \phi}{\partial x}, \quad V = AG\kappa \left(\frac{\partial u}{\partial x} - \phi \right). \quad (10)$$

We now define the dimensionless parameters $u^*(\zeta, \tau) = u(\zeta L, \tau T_T)/L$, and $T_T = L\sqrt{\frac{\rho}{G\kappa}}$, We also define the following constants

$$\alpha = \frac{AL^2}{I}, \quad \beta = \frac{AG\kappa L^2}{EI} \quad \text{and} \quad \gamma = \frac{\beta}{\alpha}.$$

Utilizing these non-dimensional parameters, the Timoshenko beam model is written as

$$\frac{\partial^2 u^*}{\partial \tau^2} = \frac{\partial^2 u^*}{\partial \zeta^2} - \frac{\partial \phi^*}{\partial \zeta}, \quad (11)$$

$$\frac{\partial^2 \phi^*}{\partial \tau^2} = \frac{1}{\gamma} \frac{\partial^2 \phi^*}{\partial \zeta^2} + \alpha \frac{\partial u^*}{\partial \zeta} - \alpha \phi^*. \quad (12)$$

Following the approach described in [17], a separation of variables of the form $u^*(\zeta, \tau) = Y^*(\tau)U^*(\zeta)$ and $\phi^*(\zeta, \tau) = Y^*(\tau)\Phi^*(\zeta)$ is considered and the resulting eigenvalue problem is given by

$$\begin{aligned} -U^{*''} + \Phi^{*'} &= \lambda U^*, \\ -\frac{1}{\gamma} \Phi^{*''} - \alpha U^{*'} + \alpha \Phi^* &= \lambda \Phi^* \end{aligned} \quad (13)$$

where λ is the non-negative eigenvalue and $\begin{bmatrix} U^* \\ \Phi^* \end{bmatrix}$ is the eigenfunction. Here $\frac{Y^{*''}}{Y^*} = -\lambda$ and $\sqrt{\lambda}$ is the non-dimensional natural frequency $\sqrt{\lambda} = \hat{\omega} T_T$, where $\hat{\omega}$ is the physical frequency predicted by the model. To solve the eigenvalue problem, the eigenfunctions are assumed to be of the form $e^{m\zeta} \mathbf{w}$ resulting in the following equation

$$\begin{bmatrix} -m^2 - \lambda & m \\ -\alpha m & -\frac{1}{\gamma} m^2 + (\alpha - \lambda) \end{bmatrix} \begin{bmatrix} w_1 \\ w_2 \end{bmatrix} = \begin{bmatrix} 0 \\ 0 \end{bmatrix}. \quad (14)$$

Equating the determinant to zero for non-trivial solutions, i.e., $m^4 + \lambda(1 + \gamma)m^2 + \gamma\lambda(\lambda\alpha) = 0$ leads to following roots of m

$$m^2 = -\frac{1}{2}\lambda(1 + \gamma)(1 \pm \Delta^{\frac{1}{2}}), \quad \text{where } \Delta = 1 - \frac{4\gamma}{(1 + \gamma)^2} \left(1 - \frac{\alpha}{\lambda}\right). \quad (15)$$

The parameter Δ in Eq. (15) is always greater than 0 but can be greater than, less than or equal to 1, depending upon whether $\lambda < \alpha$, $\lambda > \alpha$ or $\lambda = \alpha$. The three cases lead to different expressions for the mode shapes which are presented in Sections 3.1-3.3 [17]. A provides some discussion on the derivation of Eqs. (16), (17), and (18).

3.1 The case $\lambda < \alpha$

In this case m has 2 real roots denoted by $\pm\mu$ and 2 imaginary roots denoted by $\pm\omega i$. The eigenfunctions using Eq. (14) are then expressed by

$$\begin{bmatrix} U^*(\zeta) \\ \Phi^*(\zeta) \end{bmatrix} = A_1 \begin{bmatrix} \sinh \mu \zeta \\ \frac{\lambda + \mu^2}{\mu} \cosh \mu \zeta \end{bmatrix} + A_2 \begin{bmatrix} \cosh \mu \zeta \\ \frac{\lambda + \mu^2}{\mu} \sinh \mu \zeta \end{bmatrix} + A_3 \begin{bmatrix} \sin \omega \zeta \\ -\frac{\lambda - \omega^2}{\omega} \cos \omega \zeta \end{bmatrix} + A_4 \begin{bmatrix} \cos \omega \zeta \\ \frac{\lambda - \omega^2}{\omega} \sin \omega \zeta \end{bmatrix}. \quad (16)$$

3.2 The case $\lambda = \alpha$:

The roots in this case are two imaginary values denoted by $\pm\omega i$ and 0 with multiplicity 2. The eigenfunctions are then given by

$$\begin{bmatrix} U^*(\zeta) \\ \Phi^*(\zeta) \end{bmatrix} = A_1 \begin{bmatrix} 0 \\ 1 \end{bmatrix} + A_2 \begin{bmatrix} 1 \\ \alpha\zeta \end{bmatrix} + A_3 \begin{bmatrix} \sin \omega\zeta \\ -\frac{\lambda-\omega^2}{\omega} \cos \omega\zeta \end{bmatrix} + A_4 \begin{bmatrix} \cos \omega\zeta \\ \frac{\lambda-\omega^2}{\omega} \sin \omega\zeta \end{bmatrix}. \quad (17)$$

3.3 The case $\lambda > \alpha$

All the 4 roots are imaginary denoted by $\pm\theta i$ and $\pm\omega i$. The eigenfunctions are then given by

$$\begin{bmatrix} U^*(\zeta) \\ \Phi^*(\zeta) \end{bmatrix} = A_1 \begin{bmatrix} \sin \theta\zeta \\ -\frac{\lambda-\theta^2}{\theta} \cos \theta\zeta \end{bmatrix} + A_2 \begin{bmatrix} \cos \theta\zeta \\ \frac{\lambda-\theta^2}{\theta} \sin \theta\zeta \end{bmatrix} + A_3 \begin{bmatrix} \sin \omega\zeta \\ -\frac{\lambda-\omega^2}{\omega} \cos \omega\zeta \end{bmatrix} + A_4 \begin{bmatrix} \cos \omega\zeta \\ \frac{\lambda-\omega^2}{\omega} \sin \omega\zeta \end{bmatrix}. \quad (18)$$

The real quantities ω , μ (for the case $\lambda < \alpha$) and θ (for the case $\lambda > \alpha$) are given in terms of λ as [17]

$$\omega^2 = \frac{1}{2}\lambda(1+\gamma)(\Delta^{\frac{1}{2}}+1), \quad \mu^2 = \frac{1}{2}\lambda(1+\gamma)(\Delta^{\frac{1}{2}}-1), \quad \theta^2 = \frac{1}{2}\lambda(1+\gamma)(1-\Delta^{\frac{1}{2}}). \quad (19)$$

The values of the coefficients A_1 through A_4 along with the quantity λ which determines the natural frequencies depend on the specific boundary conditions and can be found by imposing the boundary conditions on the above expressions for mode shape. Figure 1 shows the most common boundary conditions, and Table 3 lists the corresponding mathematical expressions.

Condition Name	Equation 1	Equation 2
Cantilever	$u = 0$	$\phi = 0$
Simply Supported	$u = 0$	$\phi' = 0$
Free	$u' - \phi = 0$	$\phi' = 0$
Roller	$u' - \phi = 0$	$\phi = 0$

Table 3: The four standard boundary conditions for the Timoshenko beam.

4 Solution strategy for the eigenvalue problem

This section details the strategy devised for solving the eigenvalue problem. Symbolic Matlab[®] was used, as well as Mathematica[®] to perform the algebraic manipulations needed to solve the resulting system of equations. This section assumes that $\lambda > 0$, i.e., we are not concerned with rigid body modes at $\lambda = 0$ or eigenfrequencies with multiplicity 2 [23] (see Section 4.2).

The process starts by imposing the boundary conditions from Table 3 for the beam case under investigation, and using symbolic variables, we can write down a system of equations

$$\mathbf{B} \mathbf{a} = \mathbf{0}, \quad (20)$$

where the the entries of matrix \mathbf{B} are $b_{ij} = b_{ij}(\mu(\lambda), \omega(\lambda))$, where $i, j \in \{1, 2, 3, 4\}$, are obtained by applying the boundary conditions, and the entries of vector \mathbf{a} are the coefficients A_i , where $i \in \{1, 2, 3, 4\}$. It is important to first check the rank of the matrix \mathbf{B} . If \mathbf{B} is full rank, when the following process will reliably produce the needed expressions for the eigenmode coefficients. However, if \mathbf{B} is rank deficient, then the eigenvalue problem needs to be studied more closely to identify any additional constraints on the coefficients A_1 – A_4 . For all but one of the cases that we have studied the matrices had full rank. The only case with a rank deficient \mathbf{B} matrix was the pinned-pinned case with $\lambda = \alpha$. This case is described in detail in B.

After ensuring that \mathbf{B} has full rank, Gaussian elimination can then be used by choosing one of the a_i s and solving for the other entries in \mathbf{a} in terms of this a_i . However, while performing the Gaussian elimination,

it is necessary to perform column pivoting since otherwise the Gaussian elimination may not be stable [24]. Assume that after column pivoting the linear system reads

$$\tilde{\mathbf{B}} \tilde{\mathbf{a}} = \mathbf{0}, \quad (21)$$

and that we have a bijective permutation map σ from the set $\{1, 2, 3, 4\}$ onto itself such that

$$\tilde{a}_i = a_{\sigma(i)} \text{ where } i \in \{1, 2, 3, 4\}; \quad \text{and} \quad \tilde{B}_{i,j} = B_{i,\sigma(j)} \text{ where } j \in \{1, 2, 3, 4\}. \quad (22)$$

Note that the map σ is invertible, i.e., we can write $\tilde{a}_{\sigma^{-1}(i)} = a_i$ and $\tilde{B}_{i,\sigma^{-1}(j)} = B_{i,j}$. We can now use Gaussian elimination on Eq. (21) and then use Eq. (22) along with the inverse map σ^{-1} to solve for the coefficients in Eqs. (16)–(18). Since we can only solve for three of the coefficients in terms of the fourth, we choose the term \tilde{a}_4 as the free coefficient, set $\tilde{a}_4 = 1$, and find \tilde{a}_1 – \tilde{a}_3 in terms of it. This is accomplished by constructing and symbolically solving (via Gauss elimination) the augmented matrix

$$\left[\begin{array}{ccc|c} \tilde{B}_{1,\sigma(1)} & \tilde{B}_{1,\sigma(2)} & \tilde{B}_{1,\sigma(3)} & -\tilde{B}_{1,\sigma(4)} \\ \tilde{B}_{2,\sigma(1)} & \tilde{B}_{2,\sigma(2)} & \tilde{B}_{2,\sigma(3)} & -\tilde{B}_{2,\sigma(4)} \\ \tilde{B}_{3,\sigma(1)} & \tilde{B}_{3,\sigma(2)} & \tilde{B}_{3,\sigma(3)} & -\tilde{B}_{3,\sigma(4)} \end{array} \right]. \quad (23)$$

4.1 Orthonormalization of the modes

There are several choices for the orthonormalization of the modes. One of the useful choices, especially in the method of assumed modes, is to normalize the modes with respect to the beam's mass. For the Euler-Bernoulli beam this is obtained according to

$$\text{Dimensional: } \int_0^L \rho A u_i(x) u_j(x) dx = \delta_{ij}; \quad \text{Non-dimensional: } \int_0^1 \alpha U_i(\zeta) U_j(\zeta) d\zeta = \delta_{ij}, \quad (24)$$

where δ_{ij} is the Kronecker delta function.

In the case of the Timoshenko beam, one point to emphasize is that the eigenmodes are vector valued; therefore, any choice of normalization involves the inner product of two vector-valued eigenmodes. To elaborate, the mass orthonormalization for the Timoshenko model is given by

$$\text{Dimensional: } \int_0^L [\rho A U_i(x) U_j(x) + \rho I \Phi^i(x) \Phi^j(x)] dx = \delta_{ij}; \quad (25a)$$

$$\text{Non-dimensional: } \int_0^1 [U_i^*(x) U_j^*(\zeta) + \frac{1}{\alpha} \Phi_i^*(x) \Phi_j^*(\zeta)] d\zeta = \delta_{ij}. \quad (25b)$$

where U and Φ are the dimensional mode shapes and they are related to the non-dimensional mode shapes according to $U(x) = L U^*(\zeta)$ and $\Phi(x) = \Phi^*(\zeta)$, respectively. Note that these normalizations can be used for both rigid, and non-rigid beam modes. As an example, the orthonormal rigid-body modes for a free-free beam are given by

$$\begin{bmatrix} U(x) \\ \Phi(x) \end{bmatrix} = \frac{1}{\sqrt{\rho A L}} \begin{bmatrix} 1 \\ 0 \end{bmatrix}, \quad \text{and} \quad \begin{bmatrix} U(x) \\ \Phi(x) \end{bmatrix} = \frac{12}{\sqrt{\rho A L^3 + 12 \rho I L}} \begin{bmatrix} \frac{L}{2} - x \\ -1 \end{bmatrix}. \quad (26)$$

4.2 Double eigenvalues

Although double eigenvalues besides the ones corresponding to rigid body modes can theoretically occur in beam models [23], their occurrence is generally unlikely [17]. Therefore, while we are aware of the possibility of double eigenvalues, we do not consider that case in this manuscript.

5 Problem description

The standard equations for the eigenfrequencies and eigenmodes of beams having certain boundary conditions such as clamped or free ends can be numerically ill-posed in that their solution is subject to large floating point error. This can be attributed to the form of Eqs. (16) and (7) which involve differences of terms containing $\sinh(\mu\xi)$ and $\cosh(\mu\xi)$, that grow unboundedly as μ increases. These issues are manifested in both the characteristic functions and the mode shapes.

To illustrate the problem, we consider a clamped-clamped Euler-Bernoulli beam model. Fig 2a shows the characteristic function $(\cos(\mu)\cosh(\mu) - 1)$ for the dimensionless argument $\mu < 15$. The crosses are roots of this function and we see that the characteristic function appears to grow exponentially before the fifth root has been found. In fact the characteristic function will oscillate between positive and negative regions, but within an exponentially growing envelope.

Numerical instabilities also affect the normal modes. Specifically, consider the normal modes for the clamped-clamped beam

$$u_k(\zeta) = \sinh(\mu_k\zeta) - \frac{\sinh(\mu_k) - \sin(\mu_k)}{\cosh(\mu_k) - \cos(\mu_k)} \cosh(\mu_k\zeta) - \sin(\mu_k\zeta) + \frac{\sinh(\mu_k) - \sin(\mu_k)}{\cosh(\mu_k) - \cos(\mu_k)} \cos(\mu_k\zeta),$$

where μ_k is the k th root for the characteristic function. This expression shows that for large frequencies the normal modes involve small differences of large numbers which is the paradigm of numerical instability. Figure 2b illustrates this difficulty: the dashed lines are the displacements for the 25th mode as calculated using the numerically stable expression for this problem derived below - and equivalent to one of [19]. The solid line is obtained from numerical evaluation of the analytic expression above. Around $\zeta = 0.45$ Matlab[®] calculates displacements that are “NaN” and plots zeros. Figure 2 is very similar to Figure 1 of [19] and is included here for continuity and completeness.

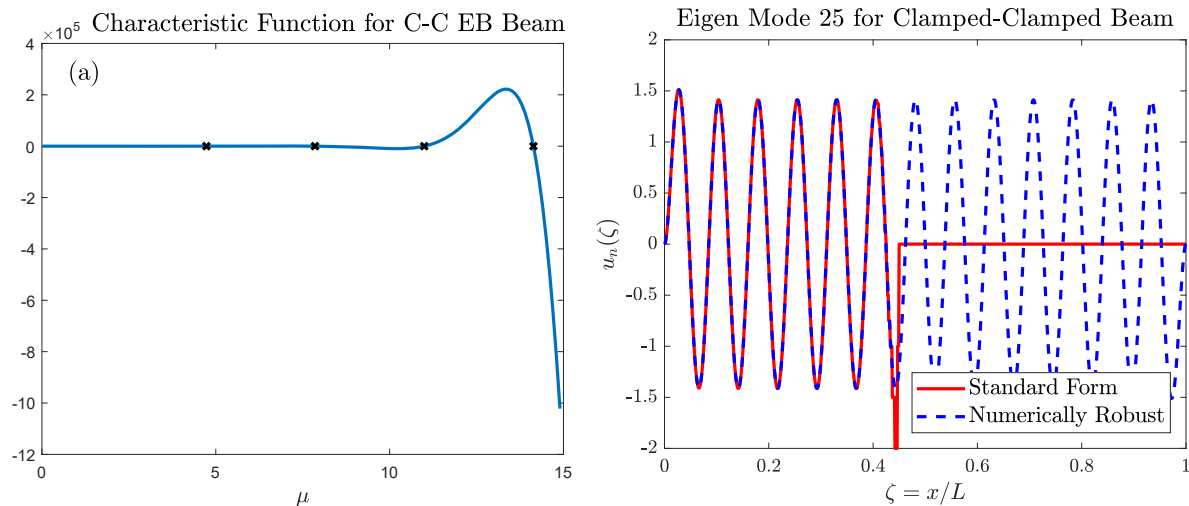


Figure 2: *Standard form of the (a) characteristic equation, and (b) of the high modes for the clamped-clamped case. The exponential growth of the hyperbolic terms leads to numerical numerical instability.*

6 Numerical stability and regularization

This section describes the numerical stabilization of the characteristic equation and the eigenmodes for the Euler-Bernoulli (Section 6.2) and Timoshenko (Section 6.3) beam models. Before the numerical stabilization method is described, Section 6.1 lists some useful identities that are used in the regularization process.

6.1 Some useful identities

Depending on the circumstances, it will be helpful to divide some equations either by $\cosh(\mu)$ or by $\sqrt{\sinh(\mu)^2 + \cosh(\mu)^2}$, so it is useful to observe that

$$1/\cosh(\mu) = \frac{2e^{-\mu}}{1+e^{-2\mu}} \rightarrow 0 \quad \text{as } \mu \rightarrow \infty, \quad (27)$$

and define

$$f(\mu) \doteq \frac{2e^{-\mu}}{1+e^{-2\mu}}. \quad (28)$$

Similarly, we observe that

$$\frac{1}{\sqrt{\sinh(\mu)^2 + \cosh(\mu)^2}} = \frac{\sqrt{2}e^{-\mu}}{\sqrt{1+e^{-4\mu}}} \rightarrow 0 \quad \text{as } \mu \rightarrow \infty, \quad (29)$$

and define

$$g(\mu) \doteq \frac{\sqrt{2}e^{-\mu}}{\sqrt{1+e^{-4\mu}}}. \quad (30)$$

We also observe that

$$\frac{\sinh(\mu)}{\sqrt{\cosh^2(\mu) + \sinh^2(\mu)}} = \frac{\sqrt{2}(1-e^{-2\mu})}{2\sqrt{1+e^{-4\mu}}} \rightarrow \frac{\sqrt{2}}{2} \quad \text{as } \mu \rightarrow \infty, \quad (31)$$

and

$$\frac{\cosh(\mu)}{\sqrt{\cosh^2(\mu) + \sinh^2(\mu)}} = \frac{\sqrt{2}(1+e^{-2\mu})}{2\sqrt{1+e^{-4\mu}}} \rightarrow \frac{\sqrt{2}}{2} \quad \text{as } \mu \rightarrow \infty. \quad (32)$$

It is now useful to define angle ψ such that

$$\psi(\mu) \doteq \text{atan2}(1-e^{-2\mu}, 1+e^{-2\mu}) \rightarrow \frac{\pi}{4} \quad \text{as } \mu \rightarrow \infty. \quad (33)$$

We can now write Eqs. (31) and (32) as

$$\frac{\sinh(\mu)}{\sqrt{\cosh^2(\mu) + \sinh^2(\mu)}} = \sin(\psi(\mu)), \quad (34)$$

and

$$\frac{\cosh(\mu)}{\sqrt{\cosh^2(\mu) + \sinh^2(\mu)}} = \cos(\psi(\mu)). \quad (35)$$

These identities are used to provide the numerically tractable forms for characteristic functions presented below.

Two other expressions that are useful in expanding the eigenmodes are

$$\frac{\sinh(\mu\zeta)}{\cosh(\mu)} = \frac{e^{-\mu(1-\zeta)} - e^{-\mu(1+\zeta)}}{1+e^{-2\mu}}, \quad \text{and} \quad \frac{\cosh(\mu\zeta)}{\cosh(\mu)} = \frac{e^{-\mu(1-\zeta)} + e^{-\mu(1+\zeta)}}{1+e^{-2\mu}}. \quad (36)$$

6.2 Numerically stable expressions for the Euler-Bernouli beam

The formulas for Euler-Bernouli beam modes have the general form shown in Eq. (7). A problem of numerical stability occurs when we consider cases of large μ (high frequency) as both $\sinh(\mu\xi)$ and $\cosh(\mu\xi)$ increase unboundedly. There has been some literature on how to address such difficulties and some good approximate methods have been developed over time. Here we present exact equivalent expressions that do not suffer from the numerical problems. As mentioned above, these stabilized expressions for the Euler Bernouli modes, are mathematically equivalent to the expressions of [19], and are presented here so that the reader may compare the EB modes with the TB modes using the same nomenclature.

Of course these difficulties occur only where A_1 or A_2 are nonzero. We first consider cases where both of these coefficients are nonzero in Section 6.2.1, while the case when these coefficients are zero is described in Section 6.2.2.

6.2.1 Case 1: non-zero A_1 and A_2

For these problems, we normalize by the first coefficient so that $A_1 = 1$. In order for the full expression of Equation 7 to stay bounded, the exponential growth of the $\sinh(\mu\xi)$ and $\cosh(\mu\xi)$ must exactly cancel. This motivates us to express

$$\frac{A_2}{A_1} = A_2 = -(1 + P(\mu)e^{-\mu}). \quad (37)$$

So

$$\begin{aligned} \sinh(\mu\zeta) + A_2 \cosh(\mu\zeta) &= \sinh(\mu\zeta) - (1 + P(\mu)e^{-\mu}) \cosh(\mu\zeta) \\ &= -e^{-\mu\zeta} - \frac{P(\mu)}{2} \left(e^{-\mu(1-\zeta)} + e^{-\mu(1+\zeta)} \right), \end{aligned} \quad (38)$$

which is well behaved as long as P is a bounded function of μ . In the type of problems discussed here A_4 is generally proportional to A_2 ($A_4 = R A_2$) so we express

$$u(\zeta) = -e^{-\mu\zeta} - \frac{P(\mu)}{2} \left(e^{-\mu(1-\zeta)} + e^{-\mu(1+\zeta)} \right) + A_3(\mu) \sin(\omega\zeta) - R(\mu) (1 + P(\mu)e^{-\mu}) \cos(\omega\zeta). \quad (39)$$

Numerically stable modal expressions are presented in Table 4. For completeness, the normal modes for less-singular configurations are also included in the table, while the roller case can be found in in Table 10 of C.

The standard form for the characteristic equations for these beam configurations is provided in the second column of Table 5. We see that in several cases, terms in the characteristic equations grow unboundedly with their argument μ . This also can lead to numerical difficulty; we would much prefer that the characteristic function (the left hand side of the characteristic equation) oscillates between bounded values, such as plus and minus 1. The characteristic equations are made numerically tractable by dividing through by $\cosh(\mu)$ or $\sqrt{\cosh^2(\mu) + \sinh^2(\mu)}$ as appropriate and employing the identities and definitions provided in Subsection 6.1. This leads to the numerically stable, scaled expressions shown in Table 5. The last column in the table shows the asymptotic values for the modes for large n .

6.2.2 Case 2: zero A_1 or A_2

We now consider the case where $A_1 = 0$ or $A_2 = 0$, which occurs for the pinned-free and pinned-pinned beams in Table 6, and all but the clamped roller cases in Table 10.

For these cases, the characteristic functions are stabilized as described in Section 6.2.1. However, we use a different normalization procedure and slightly modify the stabilization strategy for the modes in comparison to the cases considered in Section 6.2.1. Specifically, the normalization is performed according to algorithm 1.

Algorithm 1

- 1: **procedure** MODE NORMALIZATION FOR $\lambda < \alpha$
 - 2: **if** $A_1 \neq 0$ and $A_2 \neq 0$ **then**
 - 3: normalize by A_1
 - 4: **else if** $A_1 \neq 0$ and $A_2 = 0$ **then**
 - 5: normalize by the next non-zero coefficient
 - 6: **else if** $A_1 = A_3 = 0$ and $A_2 \neq 0$ and $A_4 \neq 0$ **then**
 - 7: normalize by A_4
 - 8: **else**
 - 9: normalize by the first non-zero coefficient
-

Upon normalizing the modes, we substitute their values into Eq. (7) and then we can use the equations described in Section 6.1 to numerically stabilize the modes.

Problem Definition	P	A_3	R
Clamped-Clamped	$\frac{2\sqrt{2}\cos(\mu+\frac{\pi}{4})-2e^{-\mu}}{e^{-2\mu}-2e^{-\mu}\cos(\mu)+1}$	-1	-1
Clamped-Free	$-\frac{2e^{-\mu}+2\sqrt{2}\sin(\mu+\frac{\pi}{4})}{e^{-2\mu}+2e^{-\mu}\sin(\mu)-1}$	-1	-1
Clamped-Pinned	$\frac{2\sqrt{2}\cos(\mu+\frac{\pi}{4})-2e^{-\mu}}{e^{-2\mu}-2e^{-\mu}\cos(\mu)+1}$	-1	-1
Free-Free	$\frac{2e^{-\mu}-2\sqrt{2}\sin(\mu+\frac{\pi}{4})}{-e^{-2\mu}+2e^{-\mu}\sin(\mu)+1}$	1	1
Pinned-Free	$u(\xi) = \cos(\mu) \left(\frac{e^{-\mu(1-\xi)} - e^{-\mu(1+\xi)}}{e^{-2\mu}+1} \right) + \sin(\mu\xi)$		
Pinned-Pinned	$u(\xi) = \sin(\mu\xi)$		

Table 4: Euler-Bernouli: Stabilized cases. Note that pinned-free/pinned cases do not need stabilization.

Problem Definition	Convent. Char. Eq.	Scaled Char. Eq	Asymp.
Clamped-Clamped	$\cos(\mu) \cosh(\mu) - 1 = 0$	$\cos(\mu) - f(\mu) = 0$	$(2n+1)\pi/2$
Clamped-Free	$\cos(\mu) \cosh(\mu) + 1 = 0$	$\cos(\mu) + f(\mu) = 0$	$(2n+1)\pi/2$
Clamped-Pinned	$\cosh(\mu) \sin(\mu) - \cos(\mu) \sinh(\mu) = 0$	$\sin(\mu - \psi(\mu)) = 0$	$(4n+1)\pi/4$
Free-Free	$\cos(\mu) \cosh(\mu) - 1 = 0$	$\cos(\mu) - f(\mu) = 0$	$(2n+1)\pi/2$
Pinned-Free	$\cos(\mu) \sinh(\mu) - \cosh(\mu) \sin(\mu) = 0$	$\sin(\mu - \psi(\mu)) = 0$	$(4n+1)\pi/4$
Pinned-Pinned	$\sin(\mu) = 0$	$\sin(\mu) = 0$	$n\pi$

Table 5: Euler-Bernouli: Conventional characteristic equations and their scaled form for common boundary conditions.

6.3 Numerically stable expressions for the Timoshenko beam

The equation for the modes of the Timoshenko beam with $\lambda < \alpha$ are given in Eq. (16). For simplicity, we shall set $A_1 = 1$. Section 5 discussed how when A_1 and A_2 are not zero, Eq. (16) can result in numerically unstable expressions. If we first focus on the equation for the lateral displacement of the Timoshenko beam, we obtain an expression similar to that of the Euler-Bernoulli beam shown in Eq. (7). Therefore, the numerical stability in the displacement modes $U^*(\zeta)$ can be resolved using the same procedure described in Section 6.2

We now look at the terms involved in the cross section rotation angle Φ^* for which we have the relationship

$$\cosh(\mu\zeta) + A_2 \sinh(\mu\zeta) = e^{-\mu\zeta} - \frac{P(\mu)}{2} \left(e^{-\mu(1-\zeta)} - e^{-\mu(1+\zeta)} \right), \quad (40)$$

where $P(\mu)$ is given in Table 6 for common boundary conditions, and in Table 12 of C for the roller cases. Using this relationship in the general expression for Φ^* yields

$$\begin{aligned} \Phi^* = & \left(\frac{\lambda + \mu^2}{\mu} \right) \left(e^{-\mu\zeta} - \frac{P(\mu)}{2} \left(e^{-\mu(1-\zeta)} - e^{-\mu(1+\zeta)} \right) \right) \\ & - A_3 \left(\frac{\lambda - \omega^2}{\omega} \right) \cos(\omega\zeta) - R \left(1 + P(\mu)e^{-\mu} \right) \left(\frac{\lambda - \omega^2}{\omega} \right) \sin(\omega\zeta). \end{aligned} \quad (41)$$

Therefore, using Eqs. (7) and (41)—along with Table 6 for P , A_3 , and R —gives the numerically stable modes for the lateral displacement and the cross section rotation, respectively, of the Timoshenko beam.

The characteristic equations for the Timoshenko beam can also be made numerically stable using the approach described in Section 6.2. By construction, the numerically stable forms of the characteristic func-

Problem Definition	P	A_3	R
Clamped-Clamped	$2 \frac{-e^{-\mu} + \sin(\omega) \frac{\omega(\lambda + \mu^2)}{\mu(\lambda - \omega^2)} + \cos(\omega)}{(1 + e^{-2\mu}) - 2e^{-\mu} \cos(\omega)}$	$\frac{\omega(\mu^2 + \lambda)}{\mu(\lambda - \omega^2)}$	-1
Clamped-Free	$2 \frac{(-\omega e^{-\mu}(\lambda - \omega^2) + \omega(\lambda + \mu^2) \cos(\omega) - \mu(\lambda - \omega^2) \sin(\omega))}{(\lambda - \omega^2)(\omega(e^{-2\mu} - 1) + 2\mu e^{-\mu} \sin(\omega))}$	$\frac{\omega(\mu^2 + \lambda)}{\mu(\lambda - \omega^2)}$	-1
Clamped-Pinned	$2 \frac{(-\mu e^{-\mu}(\lambda - \omega^2) + \omega(\lambda + \mu^2) \sin(\omega) + \mu(\lambda - \omega^2) \cos(\omega))}{\mu(e^{-2\mu} + 1)(\lambda - \omega^2) - 2\mu e^{-\mu}(\lambda - \omega^2) \cos(\omega)}$	$\frac{\omega(\mu^2 + \lambda)}{\mu(\lambda - \omega^2)}$	-1
Free-Free	$-2 \frac{\omega e^{-\mu}(\lambda - \omega^2) + \mu(\lambda + \mu^2) \sin(\omega) - \omega(\lambda - \omega^2) \cos(\omega)}{2\mu e^{-\mu}(\lambda + \mu^2) \sin(\omega) + \omega(e^{-2\mu} - 1)(\lambda - \omega^2)}$	$\frac{\omega}{\mu}$	$-\frac{\mu^2 + \lambda}{\lambda - \omega^2}$
Pinned-Free ^a	$U^*(\zeta) = \left(\frac{\mu \cos(\omega)}{\omega} \right) \frac{e^{-\mu(1-\zeta)} - e^{-\mu(1+\zeta)}}{1 + e^{-2\mu}} + \sin \omega \zeta$ $\Phi^*(\zeta) = \left(\frac{(\lambda + \mu^2) \cos(\omega)}{\omega} \right) \frac{e^{-\mu(1-\zeta)} + e^{-\mu(1+\zeta)}}{1 + e^{-2\mu}} - \frac{\lambda - \omega^2}{\omega} \cos \omega \zeta$		
Pinned-Pinned	$U^*(\zeta) = \sin(\omega \zeta)$ $\Phi^*(\zeta) = -\frac{\lambda - \omega^2}{\omega} \cos(\omega \zeta)$		

Table 6: Timoshenko beam: Stabilized cases.

^aNote that the published version (DOI: 10.1016/j.apacoust.2019.03.015) is missing the last term in the $\Phi^*(\zeta)$ for the pinned-free case. This is a typo that has been fixed in this arXiv version.

tions (using $\sin(\psi)$ and $\cos(\psi)$) grow at most polynomially in λ , but even that polynomial growth can be mitigated through judicious choice of normalization. For instance the conventional characteristic function for the pinned-free case is

$$\lambda \mu (\lambda + \mu^2) \sinh(\mu) \cos(\omega) + \lambda \omega (\lambda - \omega^2) \cosh(\mu) \sin(\omega). \quad (42)$$

Dividing through by $\sqrt{\cosh(\mu)^2 + \sinh(\mu)^2}$ yields

$$\lambda \mu (\lambda + \mu^2) \sin(\psi) \cos(\omega) + \lambda \omega (\lambda - \omega^2) \cos(\psi) \sin(\omega), \quad (43)$$

which we note grows polynomially in λ and its functions $\mu(\lambda)$ and $\omega(\lambda)$. For large λ , $\mu^2 \approx \lambda$ and $\omega^2 \approx \lambda$, so the above form grows approximately at $\lambda^{2.5}$. The one rigid body mode is captured through the factor λ , but for $\lambda > 0$, we may further divide through by $\lambda \sqrt{\omega \mu} (\lambda + \mu^2)$ to obtain

$$\sqrt{\mu/\omega} \sin(\psi) \cos(\omega) + \sqrt{\omega/\mu} \frac{(\lambda - \omega^2)}{(\lambda + \mu^2)} \cos(\psi) \sin(\omega) = 0 \quad (44)$$

which grows roughly as λ^0 .

For reference, Table 7 contrasts the numerically stable characteristic equations (white cells) with the conventional expressions (shaded cells) for the Timoshenko beam. Note that only the case $\lambda < \alpha$ requires the numerical stabilization.

Expressions for the characteristic functions for $\lambda < \alpha$, $\lambda = \alpha$ and $\lambda = \alpha$ for most common boundary conditions are shown in Table 8 (see C for the roller cases).

7 Results

Plots of the scaled characteristic function of the Euler Bernoulli beam for several combinations of boundary condition are shown in Figure 3. As one would expect from Table 4, scaled characteristic functions oscillate roughly between -1 and 1. The situation is a bit different for the case of the characteristic functions for the Timoshenko beam. For those cases, the scaled characteristic functions in general grow polynomially in λ for $\lambda < \alpha$ (the clamped-free case, for instance). Further division by judiciously chosen functions of λ can

Numerically stable expressions	Conventional Expressions
Clamped-Clamped	
$\sin(\psi(\mu)) \sin(\omega) \left(\frac{\omega(\lambda + \mu^2)}{\mu(\lambda - \omega^2)} - \frac{\mu(\lambda - \omega^2)}{\omega(\lambda + \mu^2)} \right) + 2 \cos(\psi(\mu)) \cos(\omega) - 2g(\mu) = 0$	$\sinh(\mu) \sin(\omega) \left(\frac{\omega(\lambda + \mu^2)}{\mu(\lambda - \omega^2)} - \frac{\mu(\lambda - \omega^2)}{\omega(\lambda + \mu^2)} \right) + 2 \cosh(\mu) \cos(\omega) - 2 = 0$
Clamped-Free	
$\left(\frac{\lambda + \mu^2}{\lambda - \omega^2} + \frac{\lambda - \omega^2}{\lambda + \mu^2} \right) \cos(\psi(\mu)) \cos(\omega) + \left(\frac{\omega}{\mu} - \frac{\mu}{\omega} \right) \sin(\psi(\mu)) \sin(\omega) - 2g(\mu) = 0$	$\left(\frac{\lambda + \mu^2}{\lambda - \omega^2} + \frac{\lambda - \omega^2}{\lambda + \mu^2} \right) \cosh(\mu) \cos(\omega) + \left(\frac{\omega}{\mu} - \frac{\mu}{\omega} \right) \sinh(\mu) \sin(\omega) - 2 = 0$
Clamped-Pinned	
$\frac{\mu(\lambda - \omega^2)}{\omega(\lambda + \mu^2)} \sin(\psi(\mu)) \cos(\omega) + \cos(\psi(\mu)) \sin(\omega) = 0$	$\frac{\mu(\lambda - \omega^2) \sinh(\mu) \cos(\omega)}{\omega(\lambda + \mu^2)} + \cosh(\mu) \sin(\omega) = 0$
Free-Free	
$-\left(\frac{\mu(\lambda + \mu^2)}{\omega(\lambda - \omega^2)} - \frac{\omega(\lambda - \omega^2)}{\mu(\lambda + \mu^2)} \right) \sin(\psi(\mu)) \sin(\omega) + 2 \cos(\psi(\mu)) \cos(\omega) - 2g(\psi) = 0$	$-\left(\frac{\mu(\lambda + \mu^2)}{\omega(\lambda - \omega^2)} - \frac{\omega(\lambda - \omega^2)}{\mu(\lambda + \mu^2)} \right) \sinh(\mu) \sin(\omega) + 2 \cosh(\mu) \cos(\omega) - 2 = 0$
Pinned-Free	
$\sqrt{\mu/\omega} \sin(\psi) \cos(\omega) + \sqrt{\omega/\mu} \frac{(\lambda - \omega^2)}{(\lambda + \mu^2)} \cos(\psi) \sin(\omega) = 0$	$\lambda\mu(\lambda + \mu^2) \sinh(\mu) \cos(\omega) + \lambda\omega(\lambda - \omega^2) \cosh(\mu) \sin(\omega) = 0$
Pinned-Pinned	
$\sin(\omega) = 0$	$(-\sin(\omega)(\mu^2 + \omega^2)^2) \sinh(\mu) = 0$

Table 7: Numerically stable and conventional (shaded) characteristic equations for $\lambda < \alpha$ the Timoshenko beam.

Clamped-Clamped	
$\lambda < \alpha$	$\lambda > \alpha$
$\sin(\psi(\mu)) \sin(\omega) \left(\frac{\omega(\lambda + \mu^2)}{\mu(\lambda - \omega^2)} - \frac{\mu(\lambda - \omega^2)}{\omega(\lambda + \mu^2)} \right) +$ $2 \cos(\psi(\mu)) \cos(\omega) - 2g(\mu)$	$\sin(\theta) \sin(\omega) \left(-\frac{\omega(\lambda - \theta^2)}{\theta(\lambda - \omega^2)} - \frac{\theta(\lambda - \omega^2)}{\omega(\lambda - \theta^2)} \right)$ $- 2 \cos(\theta) \cos(\omega) + 2$
$\lambda = \alpha: \alpha \sin \omega - \frac{2\alpha - 2\omega^2}{\omega} + \frac{2\alpha - 2\omega^2}{\omega} \cos \omega$	
Clamped-Free	
$\lambda < \alpha$	$\lambda > \alpha$
$\left(\frac{\lambda + \mu^2}{\lambda - \omega^2} + \frac{\lambda - \omega^2}{\lambda + \mu^2} \right) \cos(\psi(\mu)) \cos(\omega) +$ $\left(\frac{\omega}{\mu} - \frac{\mu}{\omega} \right) \sin(\psi(\mu)) \sin(\omega) - 2g(\mu)$	$\left(\frac{\theta^2 - \lambda}{\lambda - \omega^2} + \frac{\lambda - \omega^2}{\theta^2 - \lambda} \right) \cos(\theta) \cos(\omega) -$ $\frac{(\theta^2 + \omega^2) \sin(\theta) \sin(\omega)}{\theta \omega} + 2$
$\lambda = \alpha: (\alpha^2 - \alpha \omega^2) \sin(\omega) + 2\alpha\omega + \left(\omega^3 - 2\alpha\omega + \frac{2\alpha^2}{\omega} \right) \cos(\omega) - \frac{2\alpha^2}{\omega}$	
Clamped-Pinned	
$\lambda < \alpha$	$\lambda > \alpha$
$\frac{\mu(\lambda - \omega^2)}{\omega(\lambda + \mu^2)} \sin(\psi(\mu)) \cos(\omega) + \cos(\psi(\mu)) \sin(\omega)$	$(\omega^2 - \theta^2) \left(\sin(\theta) \cos(\omega) - \frac{\omega(\lambda - \theta^2) \cos(\theta) \sin(\omega)}{\theta(\lambda - \omega^2)} \right)$
$\lambda = \alpha: \omega^2 \sin(\omega)$	
Free-Free	
$\lambda < \alpha$	$\lambda > \alpha$
$-\left(\frac{\mu(\lambda + \mu^2)}{\omega(\lambda - \omega^2)} - \frac{\omega(\lambda - \omega^2)}{\mu(\lambda + \mu^2)} \right) \sin(\psi(\mu)) \sin(\omega) +$ $2 \cos(\psi(\mu)) \cos(\omega) - 2g(\psi)$	$\sin(\theta) \sin(\omega) \left(-\frac{\theta(\lambda - \theta^2)}{2\omega(\lambda - \omega^2)} - \frac{\omega(\lambda - \omega^2)}{2\theta(\lambda - \theta^2)} \right) -$ $\cos(\theta) \cos(\omega) + 1$
$\lambda = \alpha: -\frac{\alpha(\alpha - \omega^2)(2\alpha + \omega^3 \sin(\omega) - 2\alpha \cos(\omega) - \alpha \omega \sin(\omega))}{\omega}$	
Pinned-Free	
$\lambda < \alpha$	$\lambda > \alpha$
$\sqrt{\mu/\omega} \sin(\psi) \cos(\omega) + \sqrt{\omega/\mu} \frac{(\lambda - \omega^2)}{(\lambda + \mu^2)} \cos(\psi) \sin(\omega)$	$\frac{(\lambda - \omega^2)}{\theta} \cos(\theta) \sin(\omega) - \frac{(\lambda - \theta^2)}{\omega} \cos(\omega) \sin(\theta)$
$\lambda = \alpha: (-\omega^2 (\alpha - \omega^2)) \sin(\omega)$	
Pinned-Pinned	
$\lambda < \alpha$	$\lambda > \alpha$
$\sin(\omega)$	$\left(-\sin(\omega) (\omega^2 - \theta^2)^2 \right) \sin(\theta)$
$\lambda = \alpha: \sin(\omega)$	

Table 8: Numerically stable expressions for characteristic functions for the Timoshenko beam.

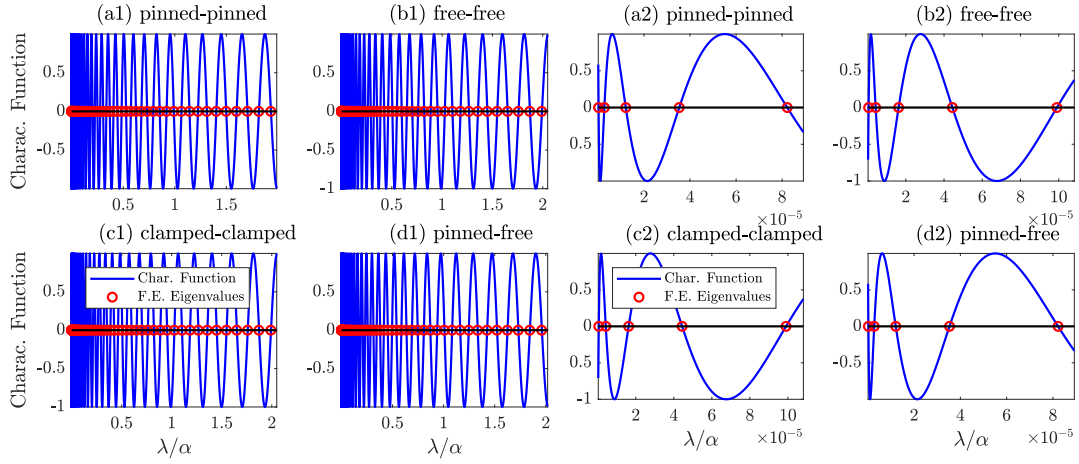


Figure 3: A plot of the characteristic function for some Euler-Bernoulli beam boundary conditions obtained using the stabilized expressions (solid line) and the eigenvalues found using finite element (circles). Plots a2–d2 are magnified versions of graphs a1–d1.

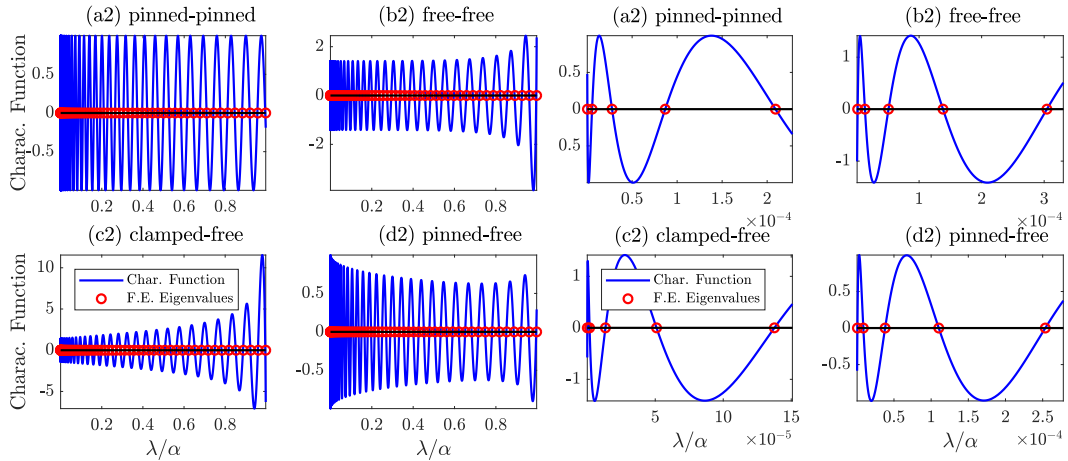


Figure 4: A plot of the characteristic function for some Timoshenko beam boundary conditions obtained using the stabilized expressions (solid line) and the eigenvalues found using finite element (circles). Plots a2–d2 are magnified versions of graphs a1–d1.

bring the the growth of the characteristic function down to something on the order of λ^0 (the case of the pinned-free Timoshenko beam.)

Numerical regularization makes all of these calculations as well as the evaluation of the modes for each case numerically well conditioned. The next section discusses a verification program where finite element analysis is used to provide confidence in the correctness of the derivations presented in this monograph and a component of this is illustrated by the red dots in the above figures; these are the eigenfrequencies obtained by finite element analysis and they do coincide very closely with the zero-crossings of the characteristic functions.

8 Verification

The derivations in the above sections lead to exact expressions for the characteristic functions and for the normal modes of Euler Bernoulli and Timoshenko beams. Though it would be good to compare these new, numerically stable forms with the original hyperbolic expressions, such comparison becomes impossible due to the numerical instability of those original expressions and to the impracticality of evaluating them. Instead, we must compare our analytic expressions to finite element results for modes and frequencies. These comparisons are not to assess accuracy (these expressions are exact), but to provide confidence that the derivations were performed correctly. Incidentally, though there exist asymptotic expressions for eigenfrequencies of Euler-Bernoulli beams at high frequencies, they do not apply to Timoshenko beams. This can be seen by observing that the eigenfrequencies of the two beam types can be expected to match only for cases of long ,thin beams at low frequencies to which the EB asymptotes do not apply.

Finite element formulations were used for the Euler-Bernoulli beam and the Timoshenko beam testing the analytic predictions for every one of the boundary condition combinations discussed above. The finite element results and the analytic expressions were compared for relative error in resonance frequency and for mutual orthonormality with respect to the finite element mass matrix of the finite element nodal degrees of freedom and the analytic solutions evaluated at the nodal locations. In all cases the error was 0.1% or less—discrepancies that can be ascribed to mesh discretization error. The very small divergence between the numerical simulations and the new analytical expressions argue that the derivations were performed accurately.

Details of this verification process are discussed in D.

9 Conclusions

The numerical difficulties associated with expressions for natural modes for Euler Bernoulli beams and with Timoshenko beams for high wave number are well known and well documented in the literature. Whereas Gonçalves et al [19] show how to overcome these problems for the case of Euler Bernoulli beams, here we generalize the approach of [19], and obtain exact but numerically tractable expressions for the eigenvalues and the eignmodes of both the Euler-Bernoulli and the Timoshenko beam models. While we tabulate the resulting numerically stable expressions for four standard boundary conditions (clamped, pinned, free, and roller), we acknowledge that are there are other important boundary conditions such as spring-supported beams. Although our approach still applies to these boundary conditions, the consideration of other boundary conditions remains a topic for future work.

Another contribution of this work is the presentation of the equations for the normal modes and the characteristic equations for beams with different boundary conditions all in the same place—and most importantly—all employing the same nomenclature. This aims to solve a recurring problem for practitioners where it is difficult to find all that information in one place. Similarly, it is generally very difficult for the practitioner to find the Euler Bernoulli beam modal expressions and characteristic equations and the expressions for the corresponding Timoshenko beam using commensurate nomenclature. This work tackles that problem as well by presenting consistent terminology, non-dimensionalizing process, and stabilization procedures for the expressions for both beam models.

References

- [1] A. Ertürk, H. Özgüven, and E. Budak, “Analytical modeling of spindle–tool dynamics on machine tools using Timoshenko beam model and receptance coupling for the prediction of tool point FRF,” *International Journal of Machine Tools and Manufacture*, vol. 46, no. 15, pp. 1901–1912, 2006.
- [2] L. Jiang and Z. Yan, “Timoshenko beam model for static bending of nanowires with surface effects,” *Physica E: Low-dimensional Systems and Nanostructures*, vol. 42, no. 9, pp. 2274 – 2279, 2010.
- [3] J. R. Claeysen, T. Tsukazan, L. Tonetto, and D. Tolfo, “Modeling the tip-sample interaction in atomic force microscopy with Timoshenko beam theory,” *Mathematics of Quantum Technologies*, vol. 2, Jan 2013.
- [4] J. A. Martin, S. C. E. Brandon, E. M. Keuler, J. R. Hermus, A. C. Ehlers, D. J. Segalman, M. S. Allen, and D. G. Thelen, “Gauging force by tapping tendons,” *Nature Communications*, vol. 9, Apr 2018.
- [5] W. Bottega, *Engineering Vibrations*. CRC Press, 2nd ed., 2014.
- [6] P. S. Timoshenko, “On the transverse vibrations of bars of uniform cross-section,” *The London, Edinburgh, and Dublin Philosophical Magazine and Journal of Science*, vol. 43, no. 253, pp. 125–131, 1922.
- [7] K. C. Le and D. M. Donskoy, “Vibrations of shells and rods,” *The Journal of the Acoustical Society of America*, vol. 109, pp. 443–443, Feb 2001.
- [8] R. W. Traill-Nash and A. R. Collar, “The effects of shear flexibility and rotatory inertia on the bending vibrations of beams,” *The Quarterly Journal of Mechanics and Applied Mathematics*, vol. 6, no. 2, pp. 186–222, 1953.
- [9] B. Abbas and J. Thomas, “The second frequency spectrum of Timoshenko beams,” *Journal of Sound and Vibration*, vol. 51, pp. 123–137, Mar 1977.
- [10] G. Bhashyam and G. Prathap, “The second frequency spectrum of Timoshenko beams,” *Journal of Sound and Vibration*, vol. 76, pp. 407–420, Jun 1981.
- [11] T. Huang, “The effect of rotatory inertia and of shear deformation on the frequency and normal mode equations of uniform beams with simple end conditions,” *Journal of Applied Mechanics*, vol. 28, no. 4, pp. 579–584, 1961.
- [12] J.-H. Kang, “An exact frequency equation in closed form for Timoshenko beam clamped at both ends,” *Journal of Sound and Vibration*, vol. 333, pp. 3332–3337, Jul 2014.
- [13] D. Young and R. P. Felgar, “Tables of characteristic functions representing normal modes of vibration of a beam,” Tech. Rep. 4913, University of Texas at Austin, 1949.
- [14] E. Dowell, “On asymptotic approximations to beam model shapes,” *Journal of applied mechanics*, vol. 51, no. 2, p. 439, 1984.
- [15] K. Shankar and A. Keane, “Energy flow predictions in a structure of rigidly joined beams using receptance theory,” *Journal of Sound and Vibration*, vol. 185, no. 5, pp. 867–890, 1995.
- [16] Y. Tang, “Numerical evaluation of uniform beam modes,” *Journal of engineering mechanics*, vol. 129, no. 12, pp. 1475–1477, 2003.
- [17] N. Van Rensburg and A. Van der Merwe, “Natural frequencies and modes of a Timoshenko beam,” *Wave motion*, vol. 44, no. 1, pp. 58–69, 2006.
- [18] P. Gonçalves, M. Brennan, and S. Elliott, “Numerical evaluation of high-order modes of vibration in uniform Euler–Bernoulli beams,” *Journal of sound and vibration*, vol. 301, no. 3, pp. 1035–1039, 2007.

- [19] P. J. P. Goncalves, A. Peplow, and M. J. Brennan, “Exact expressions for numerical evaluation of high order modes of vibration in uniform Euler-Bernoulli beams,” *Applied Acoustics*, vol. 141, pp. 371 – 373, 2018.
- [20] W. Xu, M. Cao, Q. Ren, and Z. Su, “Numerical evaluation of high-order modes for stepped beam,” *Journal of Vibration and Acoustics*, vol. 136, p. 014503, Nov 2013.
- [21] M. S. Cao, W. Xu, Z. Su, W. Ostachowicz, and N. Xia, “Local coordinate systems-based method to analyze high-order modes of N-step Timoshenko beam,” *Journal of Vibration and Control*, vol. 23, pp. 89–102, Aug 2016.
- [22] J. R. Hutchinson, “Shear coefficients for Timoshenko beam theory,” *Journal of Applied Mechanics*, vol. 68, no. 1, p. 87, 2001.
- [23] B. Geist and J. McLaughlin, “Double eigenvalues for the uniform Timoshenko beam,” *Applied Mathematics Letters*, vol. 10, no. 3, pp. 129–134, 1997.
- [24] L. N. Trefethn and I. David Bau, *Numerical linear algebra*. Siam, 1997.
- [25] R. D. Cook, D. S. Malkus, and M. E. Plesha, *Concepts and Applications of Finite Element Analysis*. New York: Wiley & Sons, third ed., 1989.
- [26] E. Hinton, T. Rock, and O. Zienkiewicz, “A note on mass lumping and related processes in the finite element method,” *Earthquake Engineering & Structural Dynamics*, vol. 4, no. 3, pp. 245–249, 1976.
- [27] Z. Friedman and J. Kosmatka, “An improved two-node Timoshenko beam finite element,” *Computers & Structures*, vol. 47, no. 3, pp. 473 – 481, 1993.

A Some Detail on Timoshenko Beam Mode Derivation

The forms of the eigenfunctions for lateral vibration of Timoshenko are provided in Eqs. (16), (17), and (18). These forms have been presented in numerous previous papers on the topic, but the reader might appreciate more discussion on the derivation of these forms than is generally available in articles, so some discussion on such derivation is presented below. We consider the cases of real eigenvalues ($m = \mu$) and of complex eigenvalues ($m = \omega$) but ignore the case of zero eigenvalue which corresponds to rigid body modes. We begin by recalling that we are looking for components of the mode that are represented by $\begin{bmatrix} U^* \\ \Phi^* \end{bmatrix} = \begin{bmatrix} w_1 e^{m\xi} \\ w_2 e^{m\xi} \end{bmatrix}$ where m is a solution to (15), the characteristic equation of the matrix in Equation Eq. (14). Because m is a solution to that characteristic equation, the rows of the matrix in Eq. (14) are proportional to each other and either row can be used to find the ratio of w_1 to w_2 ; we use the first and obtain

$$w_2/w_1 = (\lambda + m^2)/m \quad (45)$$

so our modal component is $G_1 e^{m\xi} \begin{bmatrix} 1 \\ (\lambda + m^2)/m \end{bmatrix}$

Because Eq. (15) is even in m , $-m$ is also a solution and substituting $-m$ for m in the above yields a second admissible modal component: $G_2 e^{-m\xi} \begin{bmatrix} 1 \\ -(\lambda + m^2)/m \end{bmatrix}$

Combining the contributions of both of these, we express

$$\begin{bmatrix} U^* \\ \Phi^* \end{bmatrix} = G_1 e^{m\xi} \begin{bmatrix} 1 \\ (\lambda + m^2)/m \end{bmatrix} + G_2 e^{-m\xi} \begin{bmatrix} 1 \\ -(\lambda + m^2)/m \end{bmatrix} \quad (46)$$

After some manipulation, this is hammered into the form

$$\begin{bmatrix} U^* \\ \Phi^* \end{bmatrix} = (G_1 + G_2) \begin{bmatrix} \frac{1}{2}(e^{m\xi} + e^{-m\xi}) \\ \frac{(\lambda+m^2)}{m} \frac{1}{2}(e^{m\xi} - e^{-m\xi}) \end{bmatrix} + (G_1 - G_2) \begin{bmatrix} \frac{1}{2}(e^{m\xi} - e^{-m\xi}) \\ \frac{(\lambda+m^2)}{m} \frac{1}{2}(e^{m\xi} + e^{-m\xi}) \end{bmatrix} \quad (47)$$

In the case of imaginary eigenvalues ($m = i\omega$), this becomes

$$\begin{bmatrix} U^* \\ \Phi^* \end{bmatrix} = (G_1 + G_2) \begin{bmatrix} \cos(\omega\xi) \\ \frac{(\lambda - \omega^2)}{\omega} \sin(\omega\xi) \end{bmatrix} + i(G_1 - G_2) \begin{bmatrix} \sin(\omega\xi) \\ -\frac{(\lambda - \omega^2)}{\omega} \cos(\omega\xi) \end{bmatrix} \quad (48)$$

We replace $i(G_1 - G_2)$ with C and $(G_1 + G_2)$ with D to recover the corresponding trigonometric terms in Equations 16, 17, and 18.

In the case of real eigenvalues ($m = \mu$), this becomes

$$\begin{bmatrix} U^* \\ \Phi^* \end{bmatrix} = (G_1 + G_2) \begin{bmatrix} \cosh(\mu\xi) \\ \frac{(\lambda + \mu^2)}{\mu} \sinh(\mu\xi) \end{bmatrix} + (G_1 - G_2) \begin{bmatrix} \sinh(\mu\xi) \\ \frac{(\lambda + \mu^2)}{m} \cosh(\mu\xi) \end{bmatrix} \quad (49)$$

We replace $(G_1 - G_2)$ with A and $(G_1 + G_2)$ with B to recover the corresponding hyperbolic terms in Eq. (16).

B Timoshenko beam: Pinned-pinned case

In this section, we focus on the pinned-pinned case, particularly the possible mode shapes for the case $\lambda = \alpha$. With reference to Eq. (17), the conditions that $U^*(0) = 0$, $M(0) = 0$, $U^*(1) = 0$, and $M(1) = 0$ are captured in the matrix B_1 of the coefficients A_1, A_2, A_3 , and, A_4 given by

$$B_1 = \begin{bmatrix} 0 & 1 & 0 & 1 \\ 0 & \alpha & 0 & \alpha - \omega^2 \\ 0 & 1 & \sin \omega & \cos \omega \\ 0 & \alpha & (\alpha - \omega^2) \sin \omega & (\alpha - \omega^2) \cos \omega \end{bmatrix}, \quad (50)$$

After a forward elimination with pivoting, we have

$$B_2 = \begin{bmatrix} 0 & 1 & 0 & 1 \\ 0 & 0 & 0 & -\omega^2 \\ 0 & 0 & \sin \omega & 0 \\ 0 & 0 & 0 & 0 \end{bmatrix}. \quad (51)$$

We see no dependence on α in Eq. (51), and that $\det B_2 = 0$ regardless of the value of ω . Particularly interesting is that the first column and the last row of B_2 are all zeros. If we consider the submatrix \tilde{B}_2 that excludes that row and that column we obtain

$$\tilde{B}_2 = \begin{bmatrix} 1 & 0 & 1 \\ 0 & 0 & -\omega^2 \\ 0 & \sin \omega & 0 \end{bmatrix}; \quad (52)$$

\tilde{B}_2 corresponds to the parameters A_2, A_3 , and A_4 in Eq. 17 and its determinant is $\omega^2 \sin \omega$. Back substitution yields

$$\begin{bmatrix} A_2 \\ A_3 \\ A_4 \end{bmatrix} = \begin{bmatrix} \sin \omega / \omega^2 \\ 1 \\ -\sin \omega / \omega^2 \end{bmatrix} \quad (53)$$

Since the characteristic equation is $\sin \omega = 0$, we have:

$$\begin{bmatrix} A_2 \\ A_3 \\ A_4 \end{bmatrix} = \begin{bmatrix} 0 \\ 1 \\ 0 \end{bmatrix}. \quad (54)$$

We can see from the above that the A_1 term, associated with constant ϕ , is not necessary to satisfy the boundary conditions. The question is now whether the correct solution will admit an arbitrary component of constant ϕ . To answer this question we consider the strain energy of a Timoshenko beam

$$E = \int_0^L [EI(\phi')^2 + \kappa GA(u' - \phi)^2] dx. \quad (55)$$

Let (u_c, ϕ_c) be a field that satisfies the governing equations and the boundary conditions, let E_c be the corresponding strain energy, and now consider the field $(u_c, \phi_c + A_1)$, where A_1 is a constant. When we evaluate the corresponding strain energy we obtain

$$\bar{E} = \frac{1}{2} \int_0^L [EI(\phi'_c)^2 + \kappa GA(u'_c - \phi_c - A_1)^2] dx = E_c - A_1 \kappa GA \int_0^L (u'_c - \phi_c) dx + \frac{\alpha^2 \kappa GAL}{2}. \quad (56)$$

For the case of the pinned-pinned beam, the integrand above is zero, leading to

$$\bar{E} = E_c + \frac{\alpha^2 \kappa GAL}{2}. \quad (57)$$

. The corresponding kinetic energy is

$$T = \frac{\omega_n^2}{2} \int_0^L [\rho A u^2 + \rho I \phi^2] dx = \frac{\omega_n^2}{2} \int_0^L [\rho A u_c^2 + \rho I \phi_c^2] dx + \frac{\omega_n^2 A_1^2 \rho I L}{2} = \omega_n^2 \left[\frac{M}{2} + \frac{A_1^2 \rho I L}{2} \right]. \quad (58)$$

The resulting Rayleigh quotient and its derivative with respect to A_1 are given by

$$R = \omega_n^2 = \frac{E_c + \frac{A_1^2 \kappa GAL}{2}}{\frac{M}{2} + \frac{A_1^2 \rho I L}{2}}, \quad \frac{\partial R}{\partial A_1} = 2 \left[\frac{\kappa GAL(M + A_1^2 \rho I L) - \rho I L(2E_c + A_1^2 \kappa GAL)}{(M + A_1^2 \rho I L)^2} \right] A_1 = C(A_1) A_1, \quad (59)$$

where $C(A_1) > 0$ is the function multiplying A_1 in Eq. (59). But since R must be stationary with respect to all parameters at resonance, we conclude that $A_1 = 0$.

To summarize the discussion on eigenmodes for the pinned-pinned case:

- for the case of $\lambda < \alpha$, the solution to the characteristic equation is $\sin(\omega) = 0$ so the first term in the A array is zero and the only displacement components left are $U^* = \sin(\omega\zeta)$, $\Phi^* = -((\lambda - \omega^2)/\omega) \cos(\omega\zeta)$
- for the case of $\lambda = \alpha$, the derivation above shows that the only admissible solution is the same as for $\lambda < \alpha$: $U^* = \sin(\omega\zeta)$, $\Phi^* = -((\lambda - \omega^2)/\omega) \cos(\omega\zeta)$
- For the case of $\lambda > \alpha$ the array A would be written better as

$$A = \begin{Bmatrix} \sin(\omega) \\ 0 \\ \sin(\theta) \\ 0 \end{Bmatrix}$$

The characteristic equation asserts that either $\sin(\omega) = 0$, or $\sin(\theta) = 0$ (or both equal zero, which gives a null solution.) Let's examine the two cases

1. case $\sin(\omega) = 0$ then the displacements are $U^* = \sin(\theta\zeta)$, $\Phi^* = -((\lambda - \theta^2)/\theta) \cos(\theta\zeta)$
2. case $\sin(\theta) = 0$ then the displacements are $U^* = \sin(\omega\zeta)$, $\Phi^* = -((\lambda - \omega^2)/\omega) \cos(\omega\zeta)$

C Roller boundary conditions

Problem Definition	Convent. Char. Eq.	Scaled Char. Eq	Asymp.
Pinned-Roller	$\cos(\mu) = 0$	$\cos(\mu) = 0$	$(2n + 1)\pi/2$
Clamped-Roller	$\cos(\mu) \sinh(\mu) + \cosh(\mu) \sin(\mu) = 0$	$\sin(\mu + \psi(\mu)) = 0$	$(4n - 1)\pi/4$
Roller-Free	$\cos(\mu) \sinh(\mu) + \cosh(\mu) \sin(\mu) = 0$	$\sin(\mu + \psi(\mu)) = 0$	$(4n - 1)\pi/4$
Roller-Roller	$\sin(\mu) = 0$	$\sin(\mu) = 0$	$n\pi$

Table 9: Euler-Bernoulli: Conventional characteristic equations and their numerically stabilized (scaled) form for the roller boundary conditions.

Problem Definition	P	A_3	R
Clamped-Roller	$\frac{2e^{-\mu} - 2\sqrt{2}\sin(\mu + \frac{\pi}{4})}{-e^{-2\mu} + 2e^{-\mu}\sin(\mu) + 1}$	-1	-1
Pinned-Roller	$u = \sin(\mu\xi)$		
Roller-Roller	$u = \cos(\mu\xi)$		
Roller-Free	$u = \cos(\mu) \left(\frac{e^{-\mu(1-\xi)} + e^{-\mu(1+\xi)}}{e^{-2\mu} + 1} \right) + \cos(\mu\xi)$		

Table 10: Euler-Bernoulli: stabilized roller cases. Note that only the clamped-roller case requires stabilization.

Pinned-Roller	
$\lambda < \alpha$	$\lambda > \alpha$
$\cos(\omega) \cosh(\mu)$	$\cos(\omega) \cos(\theta)$
$\lambda = \alpha: \omega^3 \cos(\omega)$	
Clamped-Roller	
$\lambda < \alpha$	$\lambda > \alpha$
$\sin(\omega) \cosh(\mu) - \frac{\omega(\lambda + \mu^2)}{\mu(\lambda - \omega^2)} \cos(\omega) \sinh(\mu)$	$\sin(\omega) \cos(\theta) - \frac{\omega(\lambda - \theta^2)}{\theta(\lambda - \omega^2)} \cos(\omega) \sin(\theta)$
$\lambda = \alpha: \sin(\omega) (\alpha - \omega^2) - \alpha \omega \cos(\omega)$	
Roller-Free	
$\lambda < \alpha$	$\lambda > \alpha$
$\sin(\omega) \cosh(\mu) - \frac{\omega(\lambda - \omega^2)}{\mu(\lambda + \mu^2)} \cos(\omega) \sinh(\mu)$	$\sin(\omega) \cos(\theta) - \frac{\omega(\lambda - \omega^2)}{\theta(\lambda - \theta^2)} \cos(\omega) \sin(\theta)$
$\lambda = \alpha: \alpha^2 \sin(\omega) + (\alpha \omega^3 - \alpha^2 \omega) \cos(\omega)$	
Roller-Roller	
$\lambda < \alpha$	$\lambda > \alpha$
$\sin(\omega) \sinh(\mu)$	$\sin(\omega) \sin(\theta)$
$\lambda = \alpha: (\alpha \omega^2) \sin(\omega)$	

Table 11: Timoshenko beam: Conventional expressions for the roller boundary condition.

Problem Definition	P	A_3	R
Clamped-Roller	$\frac{(2\omega\mu^2 + 2\lambda\omega) \cos(\omega) + (2\mu\omega^2 - 2\lambda\mu) \sin(\omega) - 2\lambda\omega e^{-\mu} - 2\mu^2\omega e^{-\mu}}{-\lambda\omega - \mu^2\omega + (2\lambda\mu e^{-\mu} - 2\mu\omega^2 e^{-\mu}) \sin(\omega) + \lambda\omega e^{-2\mu} + \mu^2\omega e^{-2\mu}}$	$\frac{\omega(\mu^2 + \lambda)}{\mu(\lambda - \omega^2)}$	-1
Pinned-Roller	$U^*(\zeta) = \sin(\omega\zeta)$ $\Phi^*(\zeta) = -\frac{\lambda - \omega^2}{\omega} \cos(\omega\zeta)$		
Roller-Free	$U^*(\zeta) = \left(\frac{\cos(\omega)(\omega^2 - \lambda)}{(\mu^2 + \lambda)} \right) \frac{e^{-\mu(1-\zeta)} + e^{-\mu(1+\zeta)}}{1 + e^{-2\mu}} + \cos(\omega\zeta)$ $\Phi^*(\zeta) = \left(\frac{\cos(\omega)(\omega^2 - \lambda)}{\mu} \right) \frac{e^{-\mu(1-\zeta)} - e^{-\mu(1+\zeta)}}{1 + e^{-2\mu}} + \frac{\lambda - \omega^2}{\omega} \sin(\omega\zeta)$		
Roller-Roller	$U^*(\zeta) = \cos(\omega\zeta)$ $\Phi^*(\zeta) = \frac{\lambda - \omega^2}{\omega} \sin(\omega\zeta)$		

Table 12: Timoshenko beam: Stabilized cases with roller boundary conditions. Note that only the clamped-roller case requires stabilization.

Numerically stable expressions	Conventional Expressions
Pinned-Roller	
$\cos(\omega) \cos(\psi(\mu))$	$\cos(\omega) \cosh(\mu)$
Clamped-Roller	
$\sin(\omega) \cos(\psi(\mu)) - \frac{\omega(\lambda + \mu^2)}{\mu(\lambda - \omega^2)} \cos(\omega) \sin(\psi(\mu))$	$\sin(\omega) \cosh(\mu) - \frac{\omega(\lambda + \mu^2)}{\mu(\lambda - \omega^2)} \cos(\omega) \sinh(\mu)$
Roller-Free	
$\sin(\omega) \cos(\psi(\mu)) - \frac{\omega(\lambda - \omega^2)}{\mu(\lambda + \mu^2)} \cos(\omega) \sin(\psi(\mu))$	$\sin(\omega) \cosh(\mu) - \frac{\omega(\lambda - \omega^2)}{\mu(\lambda + \mu^2)} \cos(\omega) \sinh(\mu)$
Roller-Roller	
$\sin(\omega) \sin(\psi(\mu))$	$\sin(\omega) \sinh(\mu)$

Table 13: Numerically stable and conventional (shaded) characteristic functions for the Timoshenko beam with roller boundary conditions and $\lambda < \alpha$. The definition for $\psi(\mu)$ can be found in Eq. (33).

D Details of the Verification Exercise

The derivations in the above sections lead to exact expressions for the characteristic functions and for the normal modes of Euler Bernoulli and Timoshenko beams. Though it would be good to compare these new, numerically stable forms with the the original hyperbolic expressions, such comparison becomes impossible due to the numerical instability of those original expressions and to the impracticality of evaluating them. Instead, we must compare our analytic expressions to finite element results for modes and frequencies. These comparisons are not to assess accuracy (these expressions are exact), but to provide confidence that the derivations were performed correctly.

D.1 The Test Case

We consider a beam that at low frequencies is approximated well by an Euler Bernoulli beam but that manifests significant shear deformation at higher frequencies, even in the $\lambda < \alpha$ regime.

We consider a steel beam of length 0.5 meters having a square cross-section dimension 1.0 cm x 1.0 cm. The material parameters are $\rho = 8050 \text{ kg/m}^3$, $E = 200 \times 10^9 \text{ Pa}$, and $G = 75 \times 10^9 \text{ Pa}$. The Timoshenko shear coefficient $\kappa = 5/6$.

D.2 Nondimensionalizing the Finite Element Solutions

One thousand elements were employed in all the finite element results reported below. Though this may seem excessive, the banded nature of the structural and stiffness matrices facilitated rapid calculation of each case. The finite element results were nondimensionalized in a manner to facilitate commensurate comparison with the analytic solutions derived in the previous section:

$$\lambda_k^N = T^2 \lambda_k^{FE} \quad U_k^N = U_k^{FE}/L \quad \text{and} \quad \Phi_k^N = \Phi_k^{FE} \quad (60)$$

where λ_k^{FE} is the k^{th} eigenvalue obtained from finite element analysis, U_k^{FE} is the displacement vector associated with the k^{th} eigenmode obtained from finite element calculation, and Φ_k^{FE} is the vector of rotations associated with the is k^{th} finite element eigenmode.

The k^{th} dimensionless eigen vector is now constructed as

$$(V_k^N)_{2i-1} = (U_k^N)_i \quad \text{and} \quad (V_k^N)_{2i} = (\Phi_k^N)_i \quad (61)$$

where $i \in (1, N_{\text{nodes}})$

The finite element mass matrix will be used to define an inner product between eigen mode arrays, but first it must be scaled to be consistent with the dimensionless eigenmode arrays defined above. Let Λ be a diagonal matrix whose elements are $[L, 1, L, 1, \dots, L, 1]$ and define

$$M_N = \Lambda M_{FE} \Lambda \quad (62)$$

where M_{FE} is the finite element mass matrix.

D.3 Orthogonality

With this new mass matrix, we define an inner product

$$(V_a, V_b) = V_a^T M_N V_b \quad (63)$$

where V_a and V_b are any real column vectors of length $2N_{\text{nodes}}$. The next step is to scale our finite element modes so that the norm of each mode is 1. By construction, the eigenmodes are mutually orthogonal, and with the normalization just mentioned we now have an orthonormal set of basis vectors:

$$(V_m^N, V_n^N) = \delta_{mn} \quad (64)$$

for any modes m and n .

Next we create the corresponding vectors from the analytic expressions for the eigenmodes.

$$(V_k^A)_{2i-1} = U^*(\lambda_k^A, \zeta_i) \quad \text{and} \quad (V_k^A)_{2i} = \Phi^*(\lambda_k^A, \zeta_i) \quad (65)$$

where λ_k^A is the k^{th} root of the characteristic equation, $\zeta_i = x_i/L$, and $\{x_i\}$ are the locations of the finite element nodes. These are also normalized so that $(V_m^A, V_m^A) = 1$ for each mode m .

If the analytic expressions for the modes jibe with the corresponding finite element modes

$$(V_m^N, V_n^A) \approx \delta_{mn} \quad (66)$$

for any modes m and n . Three natural measures of departure of the analytic and the finite element solutions are now

$$\epsilon_{\text{diag}} = \max_m |(V_m^N, V_m^A) - 1|, \quad \epsilon_{\text{off diag}} = \max_{m \neq n} |(V_m^N, V_n^A)|, \quad \text{and} \quad \epsilon_\lambda = \max_m |(\lambda_m^A - \lambda_m^N)/\lambda_m^A| \quad (67)$$

D.4 Finite Element Formulation

For Euler Bernoulli beams, the standard beam formulation (see [25]) was used, but with the element mass matrices diagonalized using the special lumping technique of Hinton et. al.[26]. For Timoshenko beams the formulation of [27] was employed.

D.5 Analytic Solution and Finite Element Comparison

The comparison of the numerically stable analytic eigen solutions for the Euler Bernoulli beam with those of the corresponding finite element analyses can be seen in Table 14. (By analytic eigen values, we mean numerical solutions to the characteristic equation.)

BC Type	Modes	ϵ_λ	ϵ_{diag}	$\epsilon_{\text{off diag}}$
Clamped-Clamped	65	0.0011	1.2e-08	8.9e-05
Clamped-Free	66	0.0027	1.1e-05	0.0026
Clamped-Pinned	65	0.0011	1.2e-08	8.7e-05
Free-Free	65	0.0014	1e-05	0.0026
Pinned-Free	65	0.0012	1e-05	0.0025
Pinned-Pinned	65	0.0011	1.8e-11	5e-06
Pinned-Roller	66	0.012	3e-07	0.00072
Clamped-Roller	65	0.0011	1.2e-08	8.6e-05
Roller-Free	65	0.0012	9.9e-06	0.0025
Roller-Roller	65	0.0011	2.5e-10	1.4e-06

Table 14: Comparison of numerically stable analytic solutions with finite element results: Euler Bernoulli beam. In each case we tested the Euler-Bernoulli beam up to roughly the same dimensionless frequency that corresponds to the Timoshenko beam. This explains the variation in the number of considered modes (either 65 or 66). In each case, for the Euler-Bernoulli beam there were more eigenvalues below the cut-off frequency obtained from the condition described above for the Timoshenko beam, i.e., we used the same criteria ($\lambda < \alpha$) even though it does not have the same physical significance in the two beam models.

The comparison of the numerically stable analytic solutions for the Timoshenko beam with those of the corresponding finite element analyses can be seen in Table 15. The very small divergence between the numerical simulations and the new analytical expressions argue that the derivations were performed accurately.

BC Type	Modes	ϵ_λ	ϵ_{diag}	$\epsilon_{\text{off diag}}$
Clamped-Clamped	63	0.0023	8.4e-05	0.00019
Clamped-Free	64	0.0022	0.00096	0.0022
Clamped-Pinned	63	0.0023	6.1e-05	0.00023
Free-Free	63	0.0022	0.0008	0.0019
Pinned-Free	63	0.0022	0.00074	0.0024
Pinned-Pinned	63	0.0024	4.5e-09	3.8e-08
Pinned-Roller	63	0.0087	6e-09	0.00011
Clamped-Roller	63	0.0023	1.4e-06	0.00016
Roller-Free	63	0.0022	2e-05	0.0016
Roller-Roller	63	0.0024	4.5e-09	1.2e-07

Table 15: Comparison of numerically stable analytic solutions with finite element results: Timoshenko beam. Note that here we consider all the modes for which $\lambda < \alpha$ in the comparison. Therefore, we go up to the 64th mode for the clamped-free boundary condition, and the 63rd mode for all the other cases.